Journal of Advanced Research in Applied Sciences and Engineering Technology

Journal homepage:
https://semarakilmu.com.my/journals/index.php/applied_sciences_eng_tech/index
ISSN: 2462-1943

Development of Landslide Risk Maps in the Rif Mountains of Morocco: Between Al Hoceïma and El Jebha

Hammouti Marwane[1,*], El Haim Mohamed[1], Mouaouiya Bensaid[1], Medini Mohammed[1], Belhadj Kamal[2]

[1] Civil, Mechanical, and Energetics Engineering Laboratory, National School of Applied Sciences of Al Hoceïma, Abdelmalek Essaâdi University, 2117 Tetouan, Morocco
[2] Applied Geosciences Laboratory, Faculty of Science, University Mohammed First, 60000 Oujda, Morocco

ABSTRACT

The Central Rif region in Morocco, from Al Jebha to Al Hoceïma, has a rich history of landslides causing significant disruptions. The recent violent earthquake of Al-Hoceïma in 2003 led to a large land movement that caused the temporary closure of Regional Road N° 610 near Kassita. Besides, winter episodes with extreme rainfall, such as the record 136 mm in March 2020 near the El Jebha town, also caused an exorbitant slope sliding that interrupted traffic on National Road N° 16. These two examples of slope sliding, among others, demonstrate the interest in understanding and managing landslide risks in this region and constitute the background of the research. Thus, the purpose of this research is to identify the most vulnerable areas to landslides in the Al Jebha and Al Hoceïma regions to support their development. To conduct this study, we followed a methodology based on the inventory of dominant soils and rock formations with their geotechnical characteristics. Then, we proceeded with the presentation of their spatial distribution in geotechnical maps, constituting the first results. Subsequently, we discussed assumptions regarding the calculation of critical angles, such as the bishop method and the height of the studied slopes, alongside the definition of calculation cases considering the effects of rainfall and seismic activity on slope stability. We then calculated the critical angle for each soil in the fourth cases defined using the Talren tool, representing the second set of results. Furthermore, we assessed the natural dips of the study area based on a Digital Elevation Model using GIS tools to compute the quantity Δ, describing the difference between the critical angle and natural dips of each soil type. This led us to define landslide risk levels based on the range of the quantity Δ. Finally, using these results, we established landslide risk maps for the fourth cases, which constitute the main result of this paper. These risk maps serve as crucial tools for government decision-makers, guiding infrastructure investments like roads and tourism toward low-risk areas, optimizing fund allocation, and enhancing landslide hazard management effectively.

Keywords:
Geotechnical engineering; ground movement; digital modelling; surveying; earthquake engineering

[*] *Corresponding author.*
E-mail address: marouan.hammouti2@gmail.com / hammouti.marwane@etu.uae.ac.ma

https://doi.org/10.37934/araset.60.1.120

1. Introduction and Contextual Overview of the Study Area

1.1 Introduction

Landslides are globally ranked seventh among major natural hazards [1] after hurricanes and earthquakes. Based on the criterion of damage caused. The Office of U.S. Foreign Disaster Assistance's databases report an average of 700 deaths per year caused by landslides [2] worldwide between 1992 and 2012. Particularly the history of landslides in Morocco [3] is quite eventful and affects various regions of the kingdom, especially in the central Rif region (between Al Jebha and Al Hoceïma). These landslides [4] cause significant material and human damage and hinder the development of the study area. Given the high potential for ground movement [5] in this area and in line with the Moroccan government's desire to promote the development of the Al Hoceïma and El Jebha region through the establishment of new port, road, and railway transport infrastructures. As well as urbanization infrastructure like electrical and potable water networks, it is prudent to select, during the preliminary phase of technical studies, locations that are shielded from the risk of landslides. This approach aims to optimize the costly maintenance of these infrastructures throughout their operational lifespan [6].

With this objective in mind, this article aims to create landslide risk maps in this study area. To do this, we conducted an inventory of the predominant surface soils and rocks [7], with their spatial representation [8] in the form of geotechnical maps with the scale of 1/500 000 using GIS tool [9], which did not exist before this work. Furthermore, we combined these geotechnical maps with topographic contour lines to identify areas where soils with weak geotechnical characteristics intersect with steep topographic gradients.

The examination of geotechnical maps indicates the prevalence of soils with low geotechnical properties [10], specifically Schist, flysch, and marl, whose critical slip angles calculated with numerical simulation using Bishop [11] Method are low (66.67% for Schist as example) in comparison to the substantial natural dip, as illustrated in the dip map. The cartographic precision of this study will be compatible with a scale of 1/500 000. The chosen reference period for the reassessment of cumulative damages is set at fifty (50) years.

It should be noted that the scope of our findings is limited due to the macro-analytical nature of the landslide phenomenon, considering the extensive study area covering approximately 17,225 km². Zoning the areas prone to landslides does not negate the necessity of conducting specific studies for each case, involving comprehensive geotechnical surveys and local monitoring with inclinometers to track landslide movements, as well as piezometers to monitor groundwater levels. Moreover, the heterogeneity of the geotechnical cross-sections and the presence of weak planes may influence assumptions regarding the shape of the landslide curve, ranging from circular to planar or any other form.

The unique aim of this work is to globally delimit areas at high risk of landslides, in order to alert decision-makers to provide monitoring stations equipped with seismographs and inclinometers to monitor the evolution of movement of large masses of unstable soil. Moreover, to plan emergency centers near these risk areas equipped with the necessary machinery to evacuate debris and ensure service to adjacent roads, as well as agglomeration centers.

1.2 Contextual Overview of the Study Area

As demonstrated by the history of ground movement incidents in the Central Rif of Morroco (Figure 1), most natural landslides have occurred either during periods of extreme rainfall or in the aftermath of violent earthquakes. Additionally, anthropogenic landslides tend to happen when road construction takes place in geotechnical challenging areas, such as those with flysch [12] or schist [13]

formations. Where Actions such as excavation and construction on slopes decrease slope stability by removing toe support of the slopes and increasing shear stress on the rupture surface, thereby reducing the safety factor. In general, the occurrence of landslides necessitates a combination of extreme rainfall, extreme natural slopes, an active seismic [14] context, and, most importantly, a geotechnical unfavorable substrate. In the following section, we will provide examples of recent slope movements in the study area.

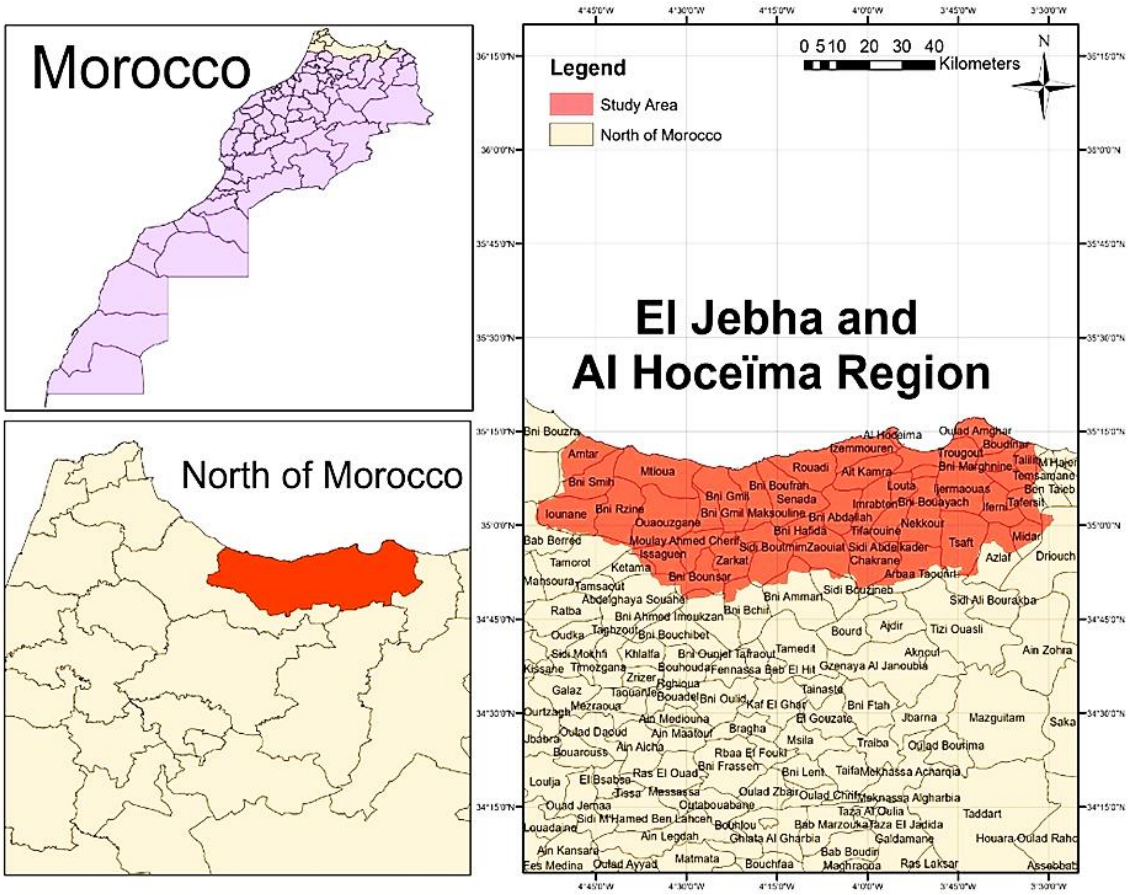

Fig. 1. Location map of the study area

1.2.1 Large-scale slope movement (Figure 2), at the embankment cut at kilometric point 190+500 on National Road N° 16 (Jebha - Amtar)

The chronological analysis of satellite images reveals a significant evolution of the landslide between 2012 and 2020. Initially, no signs of instability are visible in 2012, but retouching interventions may have triggered an initial instability. Between 2012 and 2015, the slope appears stable, but precursory signs emerge as early as the beginning of 2016. These signs persist until April 2020, when intense rains trigger mass movement affecting the lower part of the slope. Additionally, new precursory signs appear in 2020 in the western part of the slope, indicating an imminent risk of landslide in the event of further intense precipitation.

Fig. 2. Large-scale slope movement at the embankment cut on the National Road N° 16 (Jebha - Amtar)

1.2.2 Excavation of schist rock cut (Figure 3) along the Expressway Taza-Hoceïma [15] (National Road N° 02)

The causes of this landslide are attributed to lithology, predominantly consisting of schists with interbedded sandstone layers and Limestone-filled joints. These formations typically exhibit centimeter-scale bedding and locally show zones of indurated schist structured in thick beds measuring 40 to 60 cm. Structurally, the lithological section comprises beds ranging from 5 to 10 cm in thickness, characterized by a stratification oriented at North 45° and dipping at 30° to 45° towards the northwest. The section is affected by brittle deformation, marked by four main fracture families along with other secondary sub-vertical fracture planes oriented between North 35° and North 60° as shown in the Figure 4 below.

Fig. 3. Excavation of schist rock cut along the Taza-Hoceïma expressway on the National Road N° 02

These two examples of unstable terrain illustrate the challenges stemming from the absence of a map indicating where landslides could occur in the central Rif region, between Al Hoceïma and Al Jebha. Indeed, without such a map, decision-makers made a significant error in determining where to construct roads. They focused solely on efficiently moving earth, disregarding the hazards posed by the soil itself. These cases represent just a couple of instances among many others where addressing such issues results in substantial costs. If decision-makers had utilized our detailed

landslide risk map, discussed in this article, they could have saved money by making more informed decisions about where to build., thereby preventing landslide incidents and their subsequent impact on the disruption of the heavily traveled national road network used for freight and passenger transport.

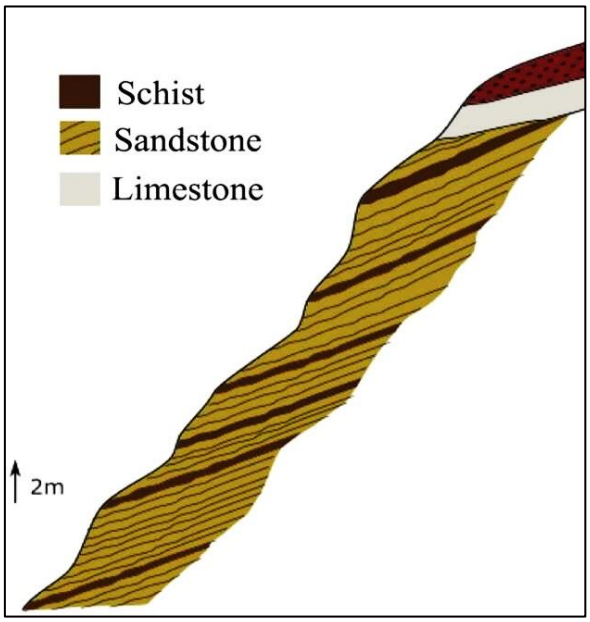

Fig. 4. lithological formations of the excavation of schist rock cut along the Expressway Taza-Hoceïma

2. Methodology

2.1 Geotechnical Data

Based on recent geotechnical surveys carried out by local geotechnical laboratories in the study we have collected a database of geotechnical data [16] necessary for the numerical modeling of the stability of the slopes as shown in the table 1 below:

Table 1
Geotechnical data of soil in Al Hoceïma and El Jebha Region

Soil nature	% Area	Average dried mass volume γ_d (t/m^3)	Atterberg liquidity limit W (%)	Average cohesion C' (kPa)	Average friction angle φ' (°)
Cretaceous marl	6.51	1.687	---	41.2	33.6
Marl-limestone	17.02	1.55	7	41.2	26.7
Limestone-sandstone	1.39	1.58	6.8	41.2	23.6
Limestone-schist	9.93	1.69	7.3	53.4	34.3
Fractured schist	2.44	2.2	---	27	26
Sand	4.67	1.8		0.1	35
Sandstone	0.03	1.52	12.8	14	18
Limestone	9.16	1.59	14.3	8	17
Clay	0.47	1.61	11.8	52	20
Schist-gneiss	1.82	2	12	40	25
Flysch	24.52	2.2	---	100	45

The data analysis reveals that Flysch occupies the largest percentage of the area (24.52%), followed by Marl-Limestone (17.02%) and Limestone-Schist (9.93%). On the other hand, Sandstone and Clay have negligible coverage percentages.

Besides, Flysch stands out with the highest average dried mass volume at 2.8 t/m³, indicating its dense composition, while Sandstone presents the lowest at 1.52 t/m³. Surprisingly, Fractured Schist shows a relatively high average dried mass volume of 2.2 t/m³, despite its lower coverage percentage, implying a dense composition. Furthermore, the data reveals that Limestone-schist demonstrates the highest average cohesion at 53.4 kPa, suggesting superior resistance to shear stress compared to other soil types. Conversely, Sand exhibits the lowest average cohesion at 0.1 kPa, indicating its minimal ability to withstand shear forces. Additionally, variations in friction angles are evident across soil types, with Sand boasting the highest at 35°. In contrast, Flysch displays a lower friction angle of 15.75°, despite its high average cohesion of 72.5 kPa, implying a trade-off between cohesion and resistance to sliding. Notably, Fractured Schist demonstrates a range for both average cohesion (26 to 32 kPa) and friction angle (24 to 27°), underscoring its heterogeneous nature and potential variability in mechanical behavior.

It should be noted that the values of geotechnical parameters are derived from laboratory tests conducted on intact samples subjected to uniform stress fields. However, most landslides occur without fully mobilizing the maximum cohesion and internal friction angle throughout the entire mass of the sliding slope, given the asymmetry of the shear stress fields mobilized along the slip curve.

2.2 Methodology Involved in Creating Geotechnical Maps

The steps involved in creating geotechnical maps using GIS tools first consist of georeferencing to the Lambert local coordinates of northern Morocco, based on the geological map already established by the Ministry of Energy and Mines. Next, we created polygonal shapefiles encompassing each area identified in the geological map, corresponding to each of the soils and rocks documented in the study area. This process resulted in the lithological map. Then, by assigning geotechnical data collected from geotechnical laboratories to each of the identified soils, we were able to represent three maps: one depicting the dried mass volume in T/m3, another illustrating the internal friction angle (ϕ) in degrees, and a third showing cohesion in kPa.

The GIS tools used is ArcMap, it is a desktop GIS application within the ArcGIS software suite, designed by Esri. It enables users to create, edit, analyze, and visualize geographic data efficiently. With a wide range of tools and functionalities, ArcMap facilitates tasks such as map creation, geoprocessing, cartography, data management, spatial analysis, and data visualization.

2.3 Topographic Data

Based on a Digital Elevation Model [17] Open source of the study area, we employed the GIS tool ArcMap to generate a digital representation of the natural land dips [18]. and this by following the last steps, the DEM data, from satellite imagery, is imported into ArcMap. Utilizing the raster processing capabilities of ArcMap, the DEM is analyzed to identify depressions or low-lying areas representing natural land dips. Through spatial analysis tools and techniques within ArcMap, these identified natural land dips are delineated and visualized on the map. As shown in Figure 5, large area has dips superior to 66 %, which is à very high amount of slope.

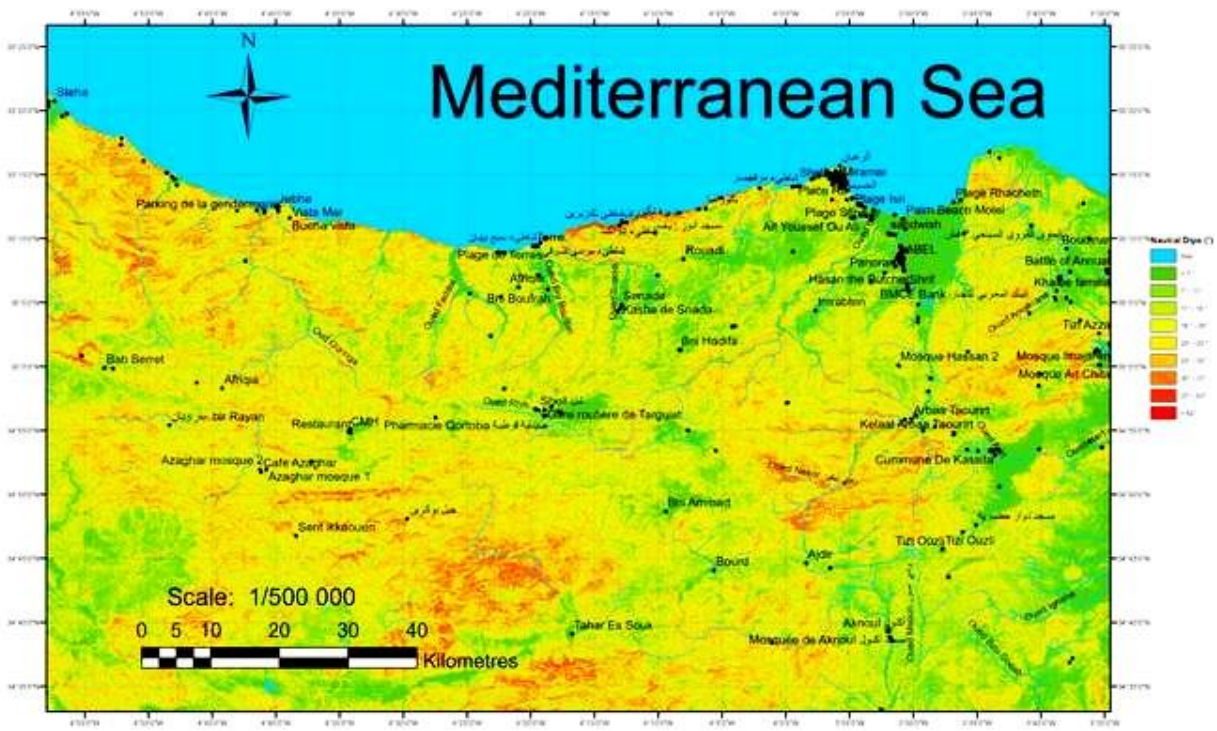

Fig. 5. Map of natural land dips of the study area

2.4 Rainfall Data

In general Water infiltration into slope soils can reduce their cohesion, thereby increasing their susceptibility to landslides Besides Water can also increase the weight of the soil, which puts additional pressure on the slope and can cause it to become unstable. Additionally, water can act as a lubricant, reducing friction between soil particles and thus facilitating movement and destabilization of the slope. Hence the need to know the quantity of rain that can water the study region, to do so, we collected rainfall (Table 2) data series from Pluviometric Stations located near the study area as the "MALHA Station", overseeing a watershed with an area of 350 square kilometers. It is situated at Moroccan Lambert coordinates (X=532,416, Y=481,744).

Table 2
Rainfall date from the Malha Station near to El Jebha region

Year	Maximum rain falls (mm)	Year	Maximum rain falls (mm)
1999	51,0	2011	63,2
2000	86,3	2012	80,8
2001	98,2	2013	62,0
2002	128,5	2014	58,2
2003	64,6	2015	25,0
2004	70,5	2016	82,0
2005	42,2	2017	57,0
2006	61,6	2018	42,3
2007	81,2	2019	75,6
2008	94,0	2020	64,9
2009	85,6	2021	31,5
2010	111,8		

However, it should be noted that the landslides observed in the study area have often occurred because of extreme rainfall events [19]. For example, in the Jebha region, about the month of March 2020, there was a daily record of approximately 136 mm of rainfall (Figure 6). This event was widespread across the entire northern part of the kingdom. Nevertheless, its epicenter coincided with the study area.

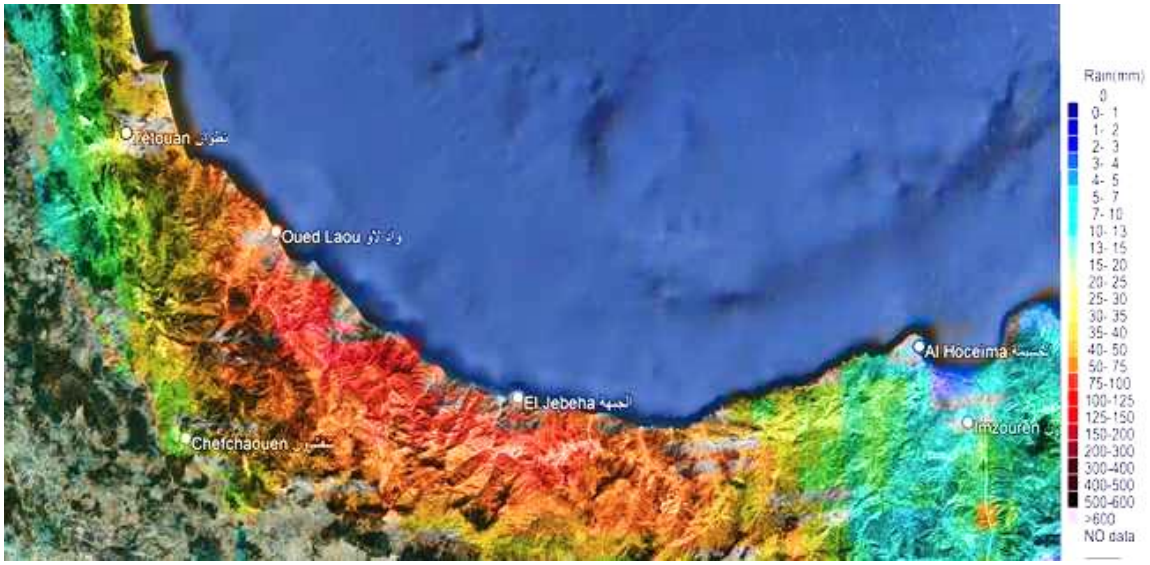

Fig. 6. Spatial distribution of daily rainfall in March 2020 around El Jebha region

2.4. Seismic Data

From a geotechnical perspective, there is a clear correlation [20] between landslide size and ground motion [21], with larger landslides associated with higher ground motion. Since a landslide occurs when the mobilized shear stress (τ) along the sliding path (circular, planar, parabolic, or any other shape) exceeds the internal shear, resistance τmax of the moving mass, this is facilitated by horizontal seismic acceleration acting on the moving soil mass. Besides it should be noted that horizontal cyclic acceleration on a slope induces horizontal inertial forces and deformations within the mass, with these deformations accumulating with each cycle. The distribution of these deformations can vary greatly, but generally, displacements concentrate near the surface in the case of unsaturated granular materials and occur deeper within the mass in the case of cohesive soils. Given the transient nature of the loading, these displacements can lead to disturbances without necessarily resulting in failure. Specifically, the slope may return to a perfectly stable state after a seismic event. The magnitude of displacements or deformations induced by an earthquake thus serves as a stability criterion that is worthwhile to quantify.

In this paper we will adopt the Pseudo-static methods for failure analysis to assess the effect of seismic action on the stability of a slope. This method is derived from the classical method of analyzing the static stability of a slope in circular failure. It assumes that in addition to the conventional gravitational body forces, there is a constant intensity body force $\gamma.\vec{k}$ intended to simulate the effect of inertia forces due to the earthquake (γ: material unit weight). In this approach, the earthquake is entirely characterized by the vector $\vec{k} = \frac{\vec{a}}{g}$ where $\vec{a}$ denotes the volumetric density of inertial acceleration. This method was introduced by Terzaghi as early as 1950 and remains widely used due to numerous developments in static analysis (Bishop method, perturbation method, etc.) [22]. The seismic vector $\vec{k}$ has two components: the horizontal seismic coefficient k_h, whose value is predominant, and the vertical seismic coefficient k_v, often neglected. For Morocco and the studied area, k_h is taken as 0.22,

whereas commonly used values for k_h range from 0.05 to 0.15 in the United States and from 0.15 to 0.25 in Japan. This choice is based on the seism maps (Figure. 7).

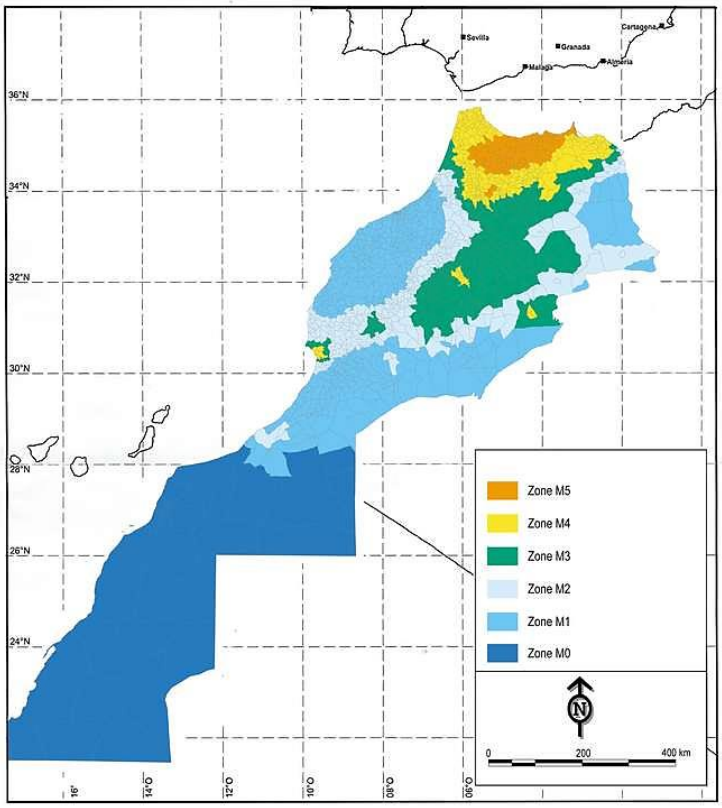

Fig. 1. Regulatory seismic map of Morocco

2.5 Assumptions of Calculation of Critical Angle

The slope failure angle will be estimated for a 20 to 40-meter-high slope by varying the width of the slope until obtaining a safety factor in the sense of the bishop method close to 1 which reflects the limit of stability of the slope (Figure 8). The choice of slope heights is justified by the rugged topography of the study area. furthermore, it is worth remembering that the Bishop Method [23] is one of several Methods of Slices developed to assess the stability of slopes and derive the associated Safety Factor. The approach differs from the Ordinary Method of slices in terms of the assumptions made regarding the interslice forces. In particular, the bishop method assumes that the shear interslice forces acting at the lateral sides of each slice i can be neglected, i.e., Vi-1 = Vi+1. It is pointed out that every method of slices requires certain assumptions to be made since the problem is, a priori, indeterminate (there are more unknown parameters than available equations).

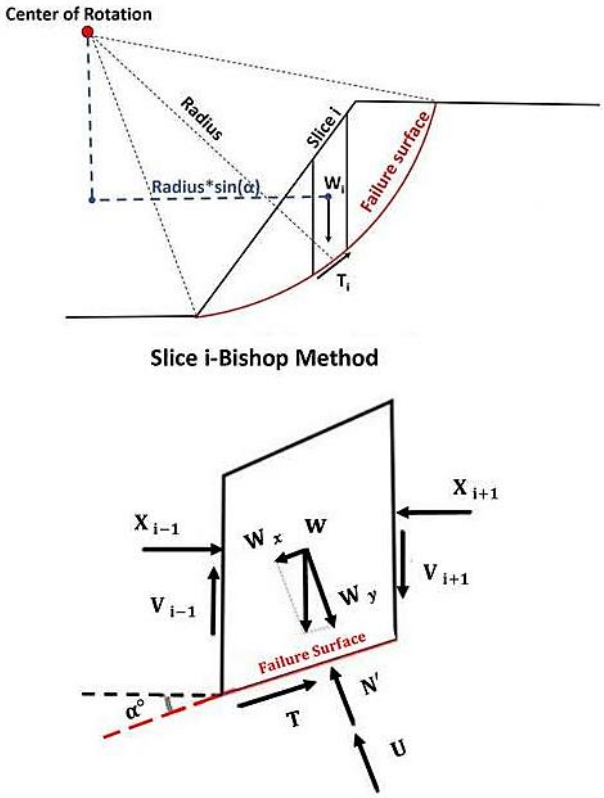

Fig. 2. The principal of Bishop Method of slices

Thus, safety of factor is written as follow:

$$\text{S. F} = \frac{\text{Resistant Moment}}{\text{Driving Moment}} = \frac{\sum_i^n T_i \times R}{\sum_i^n W_i \times R \times \sin(\alpha)} \quad (1)$$

2.6 Calculations Cases of the Critical Angle

The critical angle of a slope [24] is defined as the angle at which the risk of slope failure becomes significant. This angle is influenced by several parameters:

i. The lithological and geotechnical properties of the soil.
ii. The moisture level of the soil forming the slope, which is affected by precipitation.
iii. The occurrence or absence of seismic activity.

The search for this critical angle will be carried out following the following parametric study. First, the soil to be studied is chosen by fixing the geotechnical parameters (γ_d , C' and ϕ). Subsequently, its moisture content is fixed. Dry or Saturated state corresponding respectively to a summer or winter period (we consider only these extreme moisture states given the macro-analytical nature of the issue), which brings us to two cases: wet soil and dry soil [25]. Finally, seismic activity is taken into consideration via two scenarios such as presence or absence of seismic activity. The combination of paired scenarios brings us to four cases that we will designate as calculation scenarios, namely:

i. Case 1: Drained case without seismic activity: it illustrates the predominant scenario in the year, where the water table is at its low or non-existent level; and where seismic activity is not present.
ii. Case 2: Undrained case without seismic activity: it illustrates the scenario of the winter period in case of heavy precipitation bringing the water table to its highest level; still without seismic activity.

iii. Case 3: Drained case with seismic activity: it illustrates the accidental scenario with the consideration of seismic activity under horizontal acceleration.

iv. Case 4: Undrained case with seismic activity: it illustrates a pessimistic scenario where a reference earthquake coincides with heavy rainfall bringing the water table to its highest level; this case is unlikely, but we will treat it to highlight the combined effect of these two parameters on the critical slope of the slopes studied.

The Figure 9 summarizes the Flowchart of calculus cases of the critical angle.

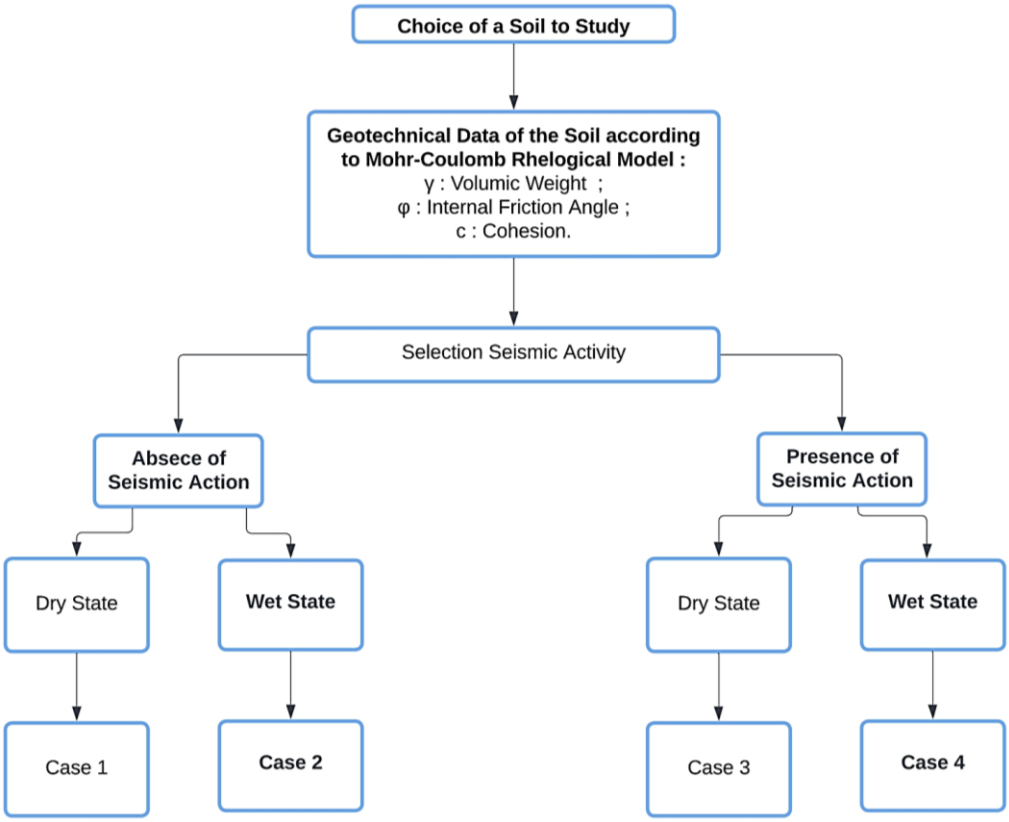

Fig. 9. Flowchart of calculus cases of the critical angle

3. Results

3.1 Result of the Critical Angle Assessment of Soil of Al Hoceïma and El Jebha Region by Talren Tool

As Explained in flow chart in Figure 10 we used Talren software, a slope stability calculation tool established by the IT company Terrasol, we evaluated the critical angle of each of the soils of the study region using the hypotheses already presented, namely the theory of bishop for the evaluation of the critical slip curve giving the lowest safety factor near to 1, and this for the fourth predefined cases to take into account the effect of rainfall and the earthquake each separately and on the other hand their mutual effect in case 4 [26]. To illustrate the modeling flowchart path, we treated the example of the critical angle model of the flysch which occupies more than 24% of the surface of the study area. It should be noted that the geotechnical data were gathered from multiple surveys carried out by local geotechnical laboratories in the study region, such as LPEE, TRECQ, which we summarized in Table 1. By following the same sequence and adopting the same calculation hypothesis for all the soils identified, we arrived at the results of the critical angles summarized in the Table 3 below. Whereas, Figure 11 shows Flysch slop critical angle.

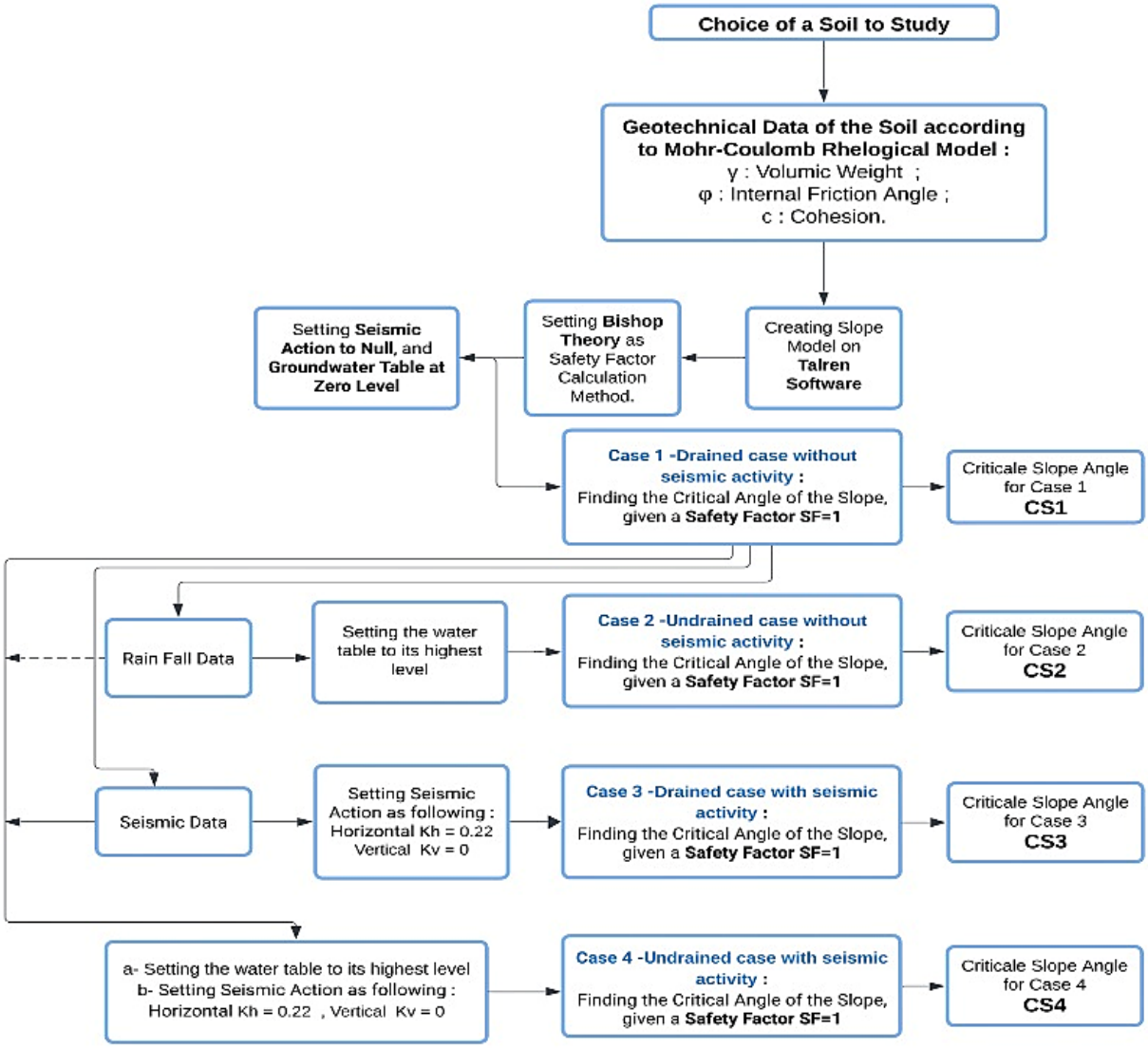

Fig. 10. Flow chart of the stage of calculation of critical angle

Table 3
Critical angles of dominant soils in Al Hoceïma and Jebha region

Soil nature	Slope high (m)	Critical angle (°) Case 1: Drained case without seismic activity	Critical angle (°) Case 2: Undrained case without seismic activity	Critical angle (°) Case 3: Drained case with seismic activity	Critical angle (°) Case 4: Undrained case with seismic activity
Greenish sandy marl	40	53.13	28.07	45	8.58
Marl-limestone	40	53.13	20.85	38.66	8.13
Limestone-sandstone	40	53.13	21.8	45	9.46
Limestone-schist	40	69.44	31.61	55	15.42
Fractured schist	20	38.66	32	29.74	10.3
Sand	20	35.53	15.42	22.83	4.96
Sandstone	20	29.74	14.2	15.94	4.08
Limestone	20	24.94	9.86	11.89	4.25
Clay	20	77.31	61.18	66.97	48.81
Schist-gneiss	40	46.46	23.96	29.74	4.76
Flysch	40	87.13	53.13	75.96	41.63

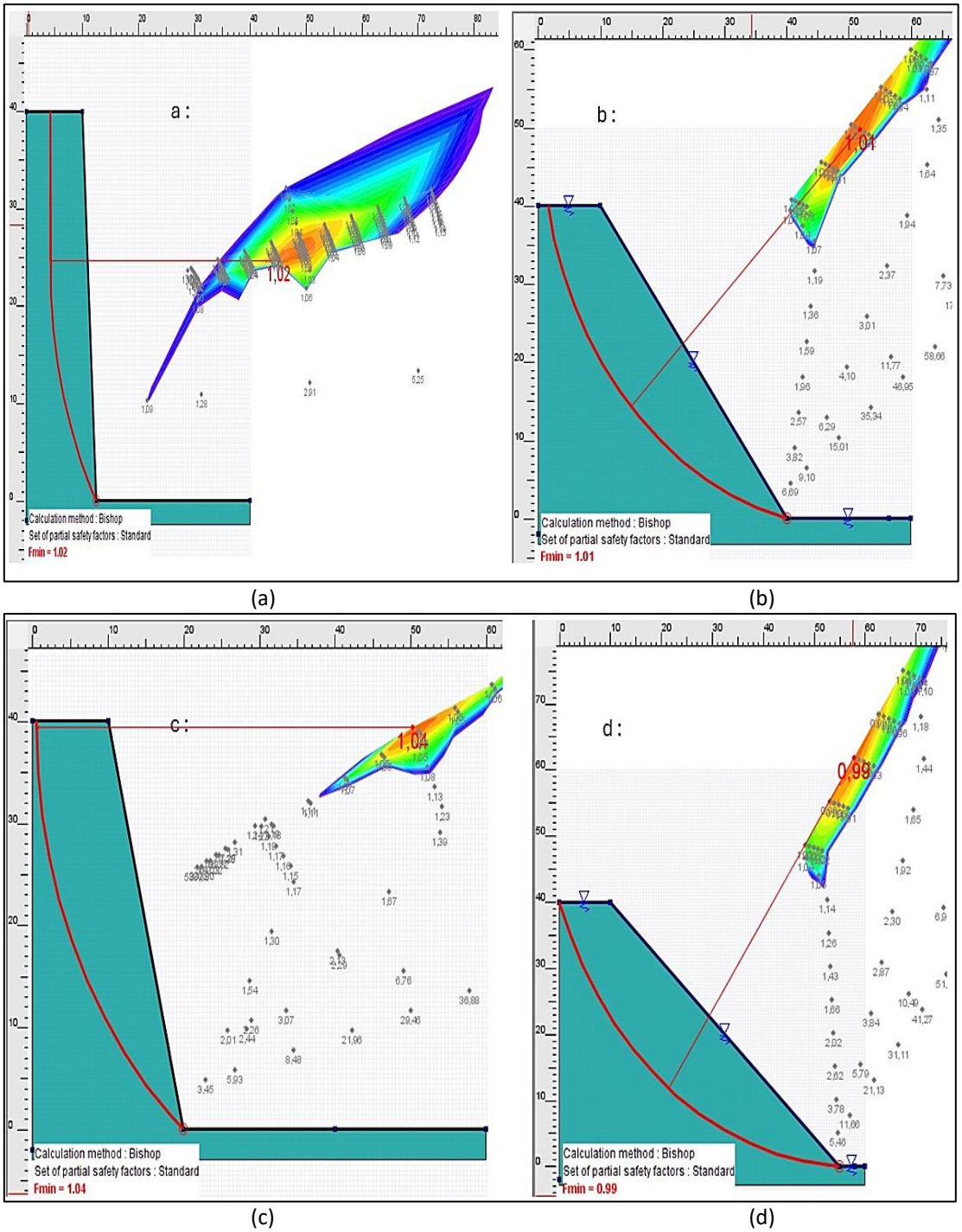

(a) (b)

(c) (d)

Fig. 3. Flysch slop critical angle (a) Case 1 (drained case without seismic activity) slope high: 40 m, wide: 2 m, critical angle: 87.13 ° (b) Case 2 (undrained case without seismic activity) slope high: 40vm, wide: 30 m, critical angle: 53.13° (c) Case 3 (drained case with seismic activity) slope high: 40 m, wide: 10 m, critical angle: 75.96° (d) Case 4 (undrained case with seismic activity) slope high 40, wide:45 m, critical angle: 41.63°

To evaluate the decay in the critical angle by the effect of the presence of rainwater and by the incidence of seismic action on the slopes, we evaluated the quantity theta (θ) defined as follows:

$$\theta = \frac{\beta case\ 1 - \beta case\ i}{\beta case\ 1} \quad (2)$$

where βcase 1 is the critical angle of a given soil for the case 1 (dominant condition over the year with no rainfall and no earthquake). B case I is the critical angle of the given soil for the case i where i∈ (2, 3, 4).

Thus, for a given case, the closer this index is to 1, the more the critical angle corresponding to this case has fallen significantly, the Figure 12 below translates into graphic form the variation of the theta (θ) quantity for the different soils identified. The qualitative analysis of the graphs below shows that case 4 is the one where the critical angle undergoes large drops, this case is cited for information only, given that the occurrence of an extreme rain event and a violent earthquake is almost zero. Moreover, the graph shows that the effect of rain (case 2) is more harmful than that of the earthquake (case 3) on the stability of the slopes of the soils subject of study.

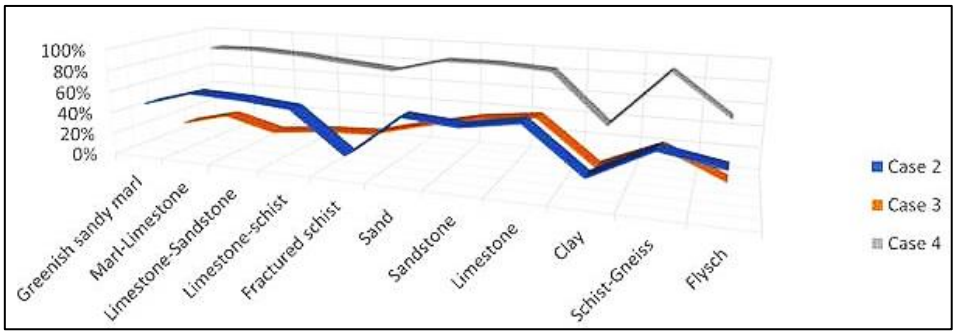

Fig. 12. Variation of the theta (θ) quantity for the different identified soils

3.2 Predictive Landslide Maps in the Middle Rif Region of Morocco – El Jebha and Al Hoceïma

Based on the slope facies map [27] besides (Figure 13), we estimated the average natural slope corresponding to each area occupied by the dominant soils previously identified. with the aim of assessing the occurrence of landslides in the study area. To do this we calculated the quantity Δ which express the difference between the natural angle of the slope and the critical angle of all the soils listed for the four calculation cases presented previously in the Figure 9.

$$\Delta \text{ case i} = \text{Natural Slop} - \text{Critical Slop case i} \quad (3)$$

where i∈ (2, 3, 4). The obtained results are summarized in the table 4 below:

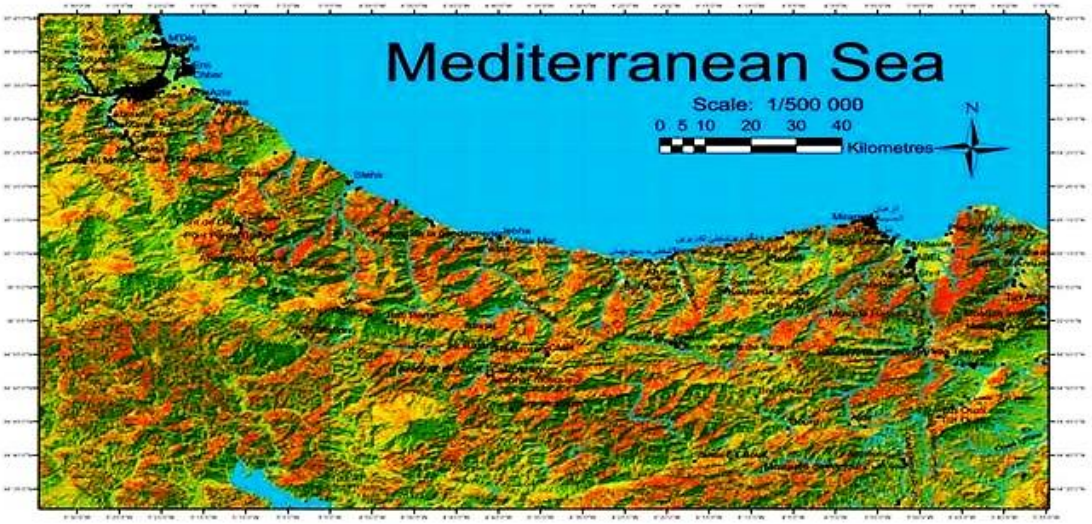

Fig. 13. Slope facies map in Al Hoceïma and El Jebha region

Table 4
The quantity Δ of dominant soils in Al Hoceïma and Jebha region

Soil nature	Slope high	Mean natural slope (°)	Case 1 No effect (natural state)	Case 2 (Rainfall effect)	Case 3 (Earthquake effect)	Case 4 (Rainfall & earthquake effect)
Greenish sandy marl	40	37.25	15.88	-9.18	7.75	-28.67
Marl-limestone	40	50.67	2.46	-29.82	-12.01	-42.54
Limestone-sandstone	40	45.81	7.32	-24.01	-0.81	-36.35
Limestone-schist	40	42.16	27.28	-10.55	12.84	-26.74
Fractured schist	20	40.86	-2.20	-8.86	-11.12	-30.56
Sand	20	41.29	-5.76	-25.87	-18.46	-36.33
Sandstone	20	35.74	-6.00	-21.54	-19.80	-31.66
Limestone	20	34.14	-9.20	-24.28	-22.25	-29.89
Clay	20	43.06	34.25	18.12	23.91	5.75
Schist-gneiss	40	56.54	-10.08	-32.58	-26.80	-51.78
Flysch	40	40.28	46.85	12.85	35.68	1.35

In order to better visualize the risk of landslides, we have defined a color gradient adapted to a risk scale ranging from a low risk to a very high risk, as shown in Table 5. By adopting this sequence of risk level, calculated on the statistical basis at equal intervals of the delta quantity whose extent is equal to a quarter of the extent Δ Max-Δ Min leading us to the following Table 6.

Table 5
Landslide Risk Level of dominant soils in Al Hoceïma and Jebha region

Slid risk level	Range of delta Δ min	Quantity Δ max
Very high risk	-51.78	-27.12
High risk	-27.12	-2.47
Medium risk	-2.47	22.19
Low risk	22.19	46.85

Table 6
Landslide Risk Level of dominant soils in Al Hoceïma and Jebha region

Soil nature	Case 1 No effect (natural state)	Case 2 Water effect	Case 3 Earthquake effect	Case 4 Water and earthquake effect
Greenish sandy marl	Medium risk	High risk	Medium risk	Very high risk
Marl-limestone	Medium risk	Very high risk	High risk	Very high risk
Limestone-sandstone	Medium risk	High risk	Medium risk	Very high risk
Limestone-schist	Low risk	High risk	Medium risk	High risk
Fractured schist	Medium risk	High risk	High risk	Very high risk
Sand	High risk	High risk	High risk	Very high risk
Sandstone	High risk	High risk	High risk	Very high risk
Limestone	High risk	High risk	High risk	Very high risk
Clay	Low risk	Medium risk	Low risk	Medium risk
Schist-gneiss	High Risk	Very high risk	High risk	Very high risk
Flysch	Low risk	Medium risk	Low risk	Medium risk

Finally, the main result of this article and which did not exist previously is the set of four landslide risk maps which delimit the areas likely to be subject to ground movements and this for the four cases taking into account of the combined effect of rain and seismic activity known to the Alhoceima and El Jebha region.

The landslide risk maps for different cases provide valuable insights into the susceptibility of the study area to landslides under various conditions. In Case 1 (natural state), it is observed that over

90% of the study area shows no susceptibility to landslides, consistent with the region's typical conditions, where landslides are predominantly associated with heavy precipitation or seismic activity (Figure 14). Moving to Case 2 (rainfall effect), the maps reveal that more than 15% of the area demonstrates a very high risk of landslides, particularly around the Jebha and Bou alma areas (Figure 15). This aligns with recent soil movement incidents, affirming the credibility of the risk maps. In Case 3 (earthquake effect), over 30% of the study area records a high risk of landslides, but no zones are classified as very high risk (Figure 16). This is justified by the tectonic history of the region, which, following past violent seismic events, has led to surface crust stability. Finally, Case 4 (rainfall & earthquake effect) highlights that more than 35% of the study area presents a very high risk of landslides (Figure 17). Although the occurrence of a severe earthquake coinciding with heavy rainfall is improbable, the maps serve as a crucial tool for guiding decision-makers in locating first-response centers near the most vulnerable areas, especially impacting towns like Al Hoceïma and El Jebha.

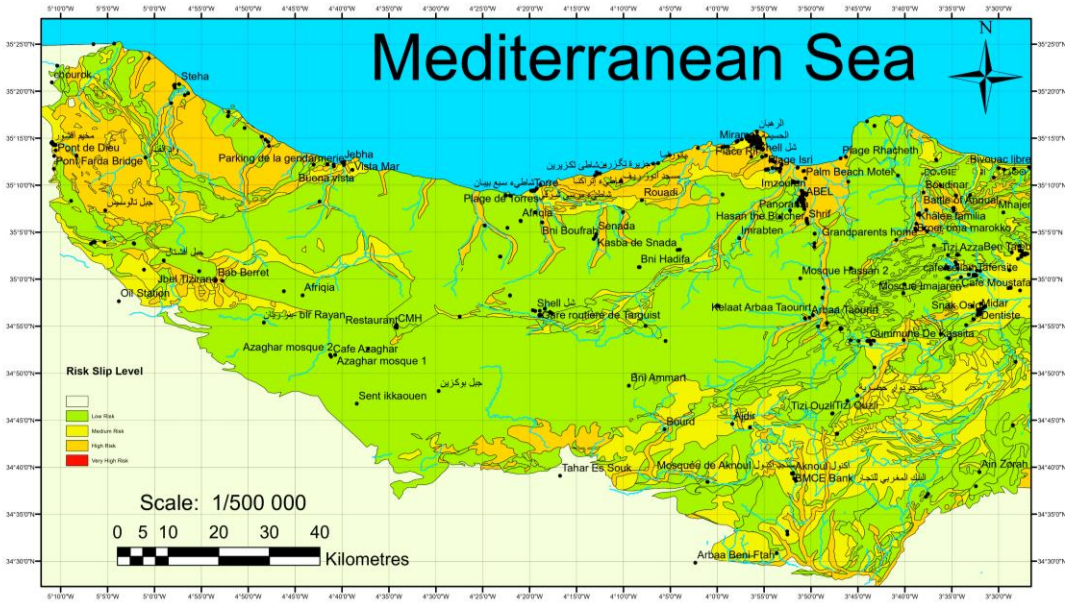

Fig. 14. Landslide risk maps for Case 1 (natural state) in Al Hoceïma and El Jebha region

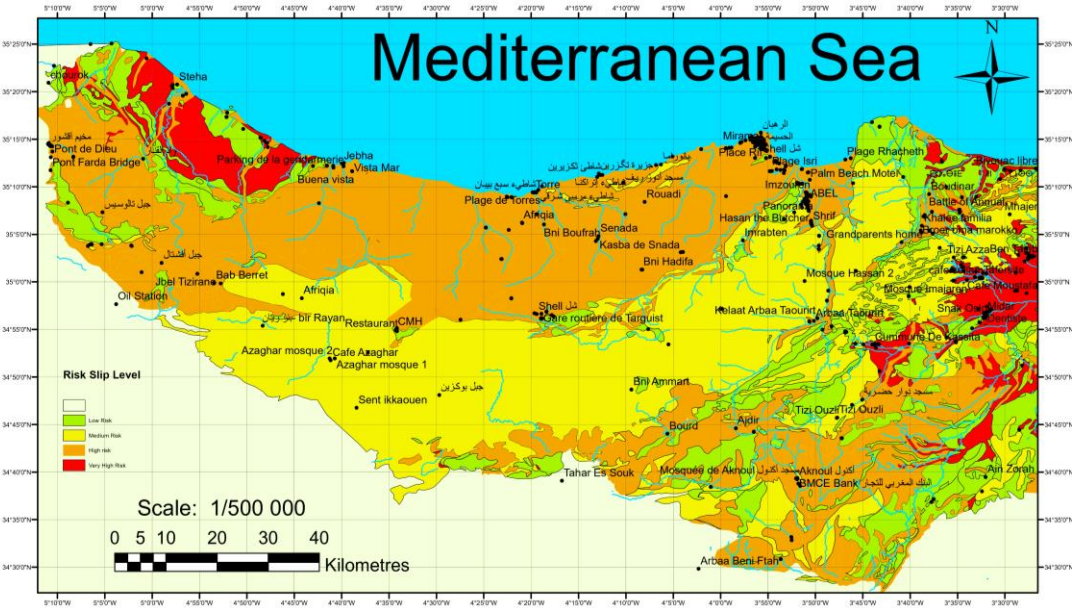

Fig. 15. Landslide Risk Maps for Case 2 (rainfall effect) in Al Hoceïma and El Jebha region

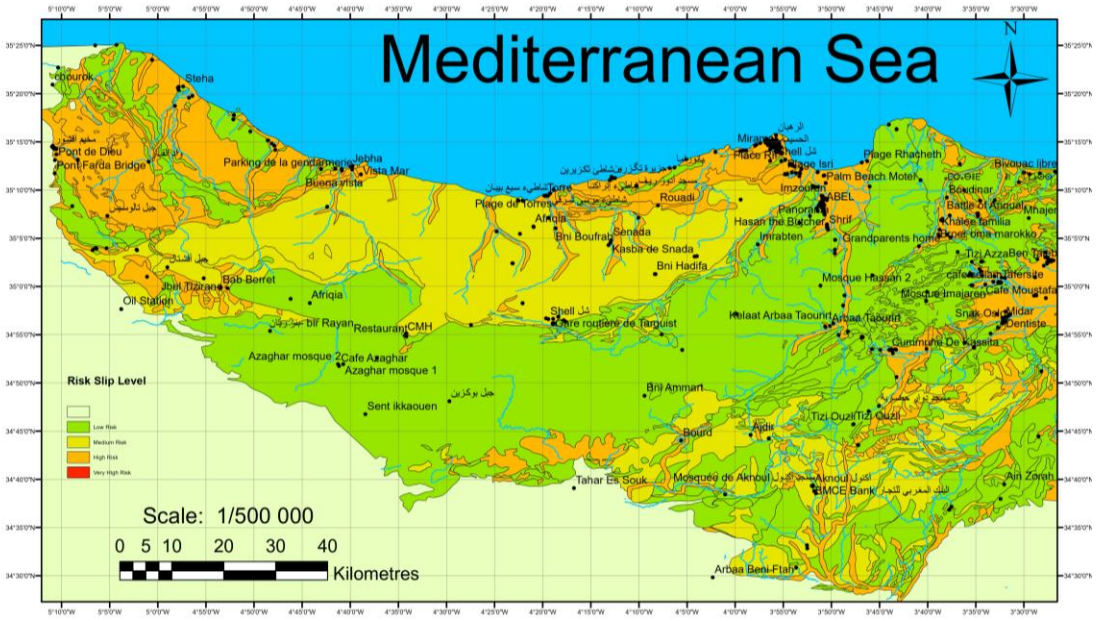

Fig. 16. Landslide risk maps for case 3 (earthquake effect) in Al Hoceïma and El Jebha region

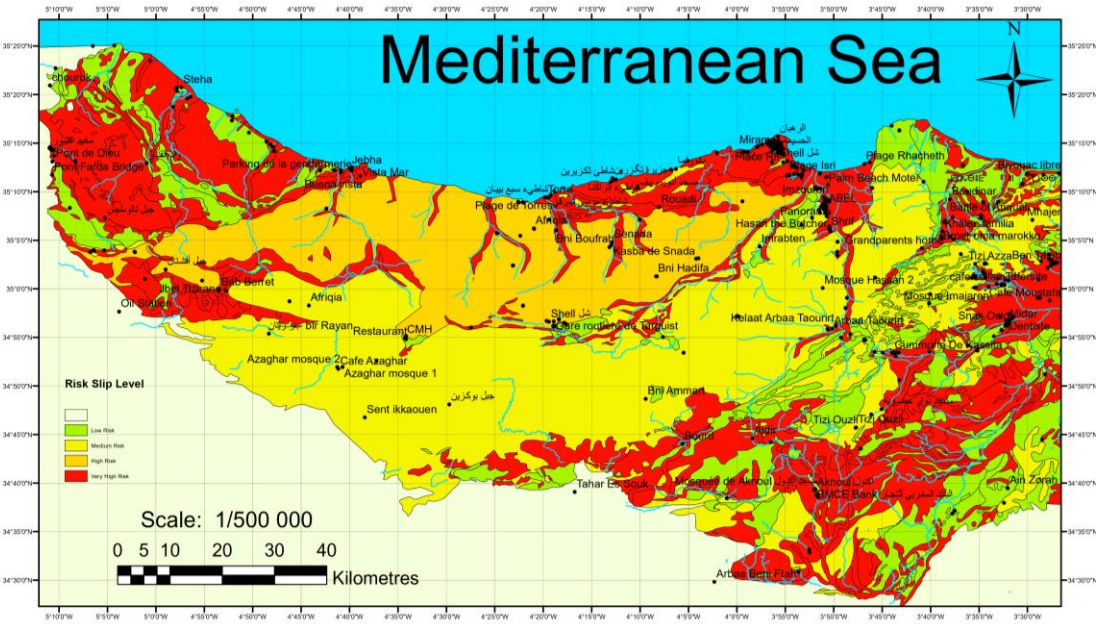

Fig. 17. Landslide risk maps for case 4 (rainfall & earthquake effect) in Al Hoceïma and El Jebha region

4. Conclusions

As a conclusion, this work led to the establishment of geotechnical maps describing the rheological parameters of the soils and rocks of the study area, which did not previously exist for this region of the Middle Rif in the Kingdom of Morocco. all the more we have identified 2 parameters significantly affecting the stability of the slopes in this region, namely the rainfall and the seismicity of the bedrock, thus, to take into account their effect separately on the critical angle of the slopes we have introduced four cases of calculation such that case 1 reflects the natural state of the slopes, that is to say without the presence of a water table fed by precipitation and without seismic action. while case 2 takes into account the effect of rainfall by bringing the water table to its highest level,

i.e. a state of full saturation of soil, while the 3rd case only takes into account the presence of seismic action via a horizontal acceleration estimated at 0.22g where g is the acceleration of gravity, finally case 4 takes into account the simultaneous effect of a torrential rain and a violent earthquake, it is cited for information purposes being given that the probability of occurrence of this event is almost zero.

Thanks to this division of cases, we arrived at results illustrating the incidence of the drastic effect of rain on the critical angle which reduces internal cohesion by lubricating the aggregates and increases the weight of the slope subject to sliding. Furthermore, to better illustrate the areas with high landslide risk in the region of Al Hoceïma and Al Jebha, we have established landslide risk maps which could be of great use to government decision-makers regarding investment in infrastructure such as roads, sanitation and drinking water supply networks, tourist infrastructure, hotels and maritime terminals given the tourist and agricultural character of the region.

These risk maps make it possible to assess that more than 15% of the study area is susceptible to the risk of landslides during a rainfall period. This innovative result will guide decision-makers to avoid these areas in future infrastructure implementations. In the meantime, we plan to offer a range of stabilization solutions best suited to the geotechnical context of the Alhoceima and El Jebha area.

Acknowledgement
The corresponding author is grateful to the laboratory of LPEE and TRECQ for providing the valuable geotechnical data of dominant soil in Al Hoceïma and El Jebha Region.

References

[1] Winter, Mike G., Barbara Shearer, Derek Palmer, David Peeling, Clare Harmer, and Jonathan Sharpe. "The economic impact of landslides and floods on the road network." *Procedia Engineering* 143 (2016): 1425-1434. https://doi.org/10.1016/j.proeng.2016.06.168

[2] AbdelRahman, Mohamed AE. "Remote sensing and geographic information system for soil analysis—vulnerability mapping and assessment." In *Geoinformatics for Geosciences*, pp. 309-324. Elsevier, 2023. https://doi.org/10.1016/B978-0-323-98983-1.00018-1

[3] Es-smairi, Abderrazzak, Brahim Elmoutchou, Riyaz Ahmad Mir, Abdelouahed El Ouazani Touhami, and Mustapha Namous. "Delineation of landslide susceptible zones using Frequency Ratio (FR) and Shannon Entropy (SE) models in northern Rif, Morocco." *Geosystems and Geoenvironment* 2, no. 4 (2023): 100195. https://doi.org/10.1016/j.geogeo.2023.100195

[4] Chen, Songchao, Dominique Arrouays, Vera Leatitia Mulder, Laura Poggio, Budiman Minasny, Pierre Roudier, Zamir Libohova et al. "Digital mapping of GlobalSoilMap soil properties at a broad scale: A review." *Geoderma* 409 (2022): 115567. https://doi.org/10.1016/j.geoderma.2021.115567

[5] Merry, Krista, Pete Bettinger, Michael Crosby, and Kevin Boston. *Geographic information system skills for foresters and natural resource managers*. Elsevier, 2022.

[6] Chen, Jiao, Shenghao Ai, Jia Liu, Hang Yang, Li Wang, Mengke Zhu, Dongqing Fu, Siqian Yang, Xiaoyan Ai, and Yingwei Ai. "The life span and influencing factors of metal mesh in artificial soil on railway rock-cut slopes in humid areas." *Science of the Total Environment* 671 (2019): 41-51. https://doi.org/10.1016/j.scitotenv.2019.03.284

[7] Youssef, Bammou, Ismail Bouskri, Benzougagh Brahim, Shuraik Kader, Igmoullan Brahim, Bensaid Abdelkrim, and Velibor Spalević. "The contribution of the frequency ratio model and the prediction rate for the analysis of landslide risk in the Tizi N'tichka area on the national road (RN9) linking Marrakech and Ouarzazate." *Catena* 232 (2023): 107464. https://doi.org/10.1016/j.catena.2023.107464

[8] Sivakumar, Vidhya Lakshmi, Rakshith Radha Krishnappa, and Manoj Nallanathel. "Drought vulnerability assessment and mapping using Multi-Criteria decision making (MCDM) and application of Analytic Hierarchy process (AHP) for Namakkal District, Tamilnadu, India." *Materials Today: Proceedings* 43 (2021): 1592-1599. https://doi.org/10.1016/j.matpr.2020.09.657

[9] Guettouche, Amar. "Using a GIS to assess the land movements hazard: application on Berhoum Area, Hodna Basin, Algeria." *Journal of Geographic Information System* 11, no. 2 (2019): 166-184. https://doi.org/10.4236/jgis.2019.112012

[10] Robbins, B.A., I.J. Stephens, and W.F. Marcuson. "Geotechnical engineering." *Encyclopedia of Geology (Second Edition)* (2021): 377–92. https://doi.org/10.1016/B978-0-12-409548-9.12508-4
[11] Berli, Markus, and Paul D. Hallett. "Soil mechanics." *Encyclopedia of Soils in the Environment (Second Edition)* 5 (2023): 69-84. https://doi.org/10.1016/B978-0-12-822974-3.00283-4
[12] Atouabat, Achraf, Sveva Corrado, Andrea Schito, Faouziya Haissen, Oriol Gimeno-Vives, Geoffroy Mohn, and Dominique Frizon de Lamotte. "Validating structural styles in the Flysch Basin Northern Rif (Morocco) by means of thermal modeling." *Geosciences* 10, no. 9 (2020): 325. https://doi.org/10.3390/geosciences10090325
[13] Cherifi, Hicham, Abdel-Ali Chaouni, Ghizlane Fattah, Abdessamad Jalouni, Imane Jabri, Hicham El Asmi, and Imad Raini. "Physico-mechanical characterization of schists in Tazzeka complex [Taza Province, Eastern Morocco]." *Case Studies in Construction Materials* 15 (2021): e00692. https://doi.org/10.1016/j.cscm.2021.e00692
[14] Tahayt, Abdelilah, K. L. Feigl, Taoufik Mourabit, Alexis Rigo, Robert Reilinger, Simon McClusky, Abdeladi Fadil et al. "The Al Hoceima (Morocco) earthquake of 24 February 2004, analysis and interpretation of data from ENVISAT ASAR and SPOT5 validated by ground-based observations." *Remote Sensing of Environment* 113, no. 2 (2009): 306-316. https://doi.org/10.1016/j.rse.2008.09.015
[15] Cherifi, Hicham, Abdel-Ali Chaouni, Mohamed Ettayeb, Imane Jabri, Hicham El-Asmi, Imad Raini, and Imane Raini. "Management of rock hazard: Case of the schistose excavation D8, Taza-Al Hoceima expressway, Morocco." *Arabian Journal of Geosciences* 15, no. 11 (2022): 1030. https://doi.org/10.1007/s12517-022-10316-x
[16] Komadja, Gbétoglo Charles, Sarada Prasad Pradhan, Afolayan David Oluwasegun, Amulya Ratna Roul, Tido Tiwa Stanislas, Raoul Adéniyi Laïbi, Babatunde Adebayo, and Azikiwe Peter Onwualu. "Geotechnical and geological investigation of slope stability of a section of road cut debris-slopes along NH-7, Uttarakhand, India." *Results in Engineering* 10 (2021): 100227. https://doi.org/10.1016/j.rineng.2021.100227
[17] Cebulski, Jarosław, Bernadetta Pasierb, Dariusz Wieczorek, and Artur Zieliński. "Reconstruction of landslide movements using digital elevation model and electrical resistivity tomography analysis in the Polish Outer Carpathians." *Catena* 195 (2020): 104758. https://doi.org/10.1016/j.catena.2020.104758
[18] Saritha, G., T. Saravanan, K. Anbumani, and J. Surendiran. "Digital elevation model and terrain mapping using LiDAR." *Materials Today: Proceedings* 46 (2021): 3979-3983. https://doi.org/10.1016/j.matpr.2021.02.525
[19] Ji, Jian, Tong Zhang, Hongzhi Cui, Xin Yin, and Weijie Zhang. "Numerical investigation of post-earthquake rainfall-induced slope instability considering strain-softening effect of soils." *Soil Dynamics and Earthquake Engineering* 171 (2023): 107938. https://doi.org/10.1016/j.soildyn.2023.107938
[20] Sridharan, Aadityan, and Sundararaman Gopalan. "Correlations among properties of lithological units that contribute to earthquake induced landslides." *Materials Today: Proceedings* 33 (2020): 2402-2406. https://doi.org/10.1016/j.matpr.2020.07.265
[21] Chen, You-Liang, Geng-Yun Liu, Ning Li, Xi Du, Su-Ran Wang, and Rafig Azzam. "Stability evaluation of slope subjected to seismic effect combined with consequent rainfall." *Engineering Geology* 266 (2020): 105461. https://doi.org/10.1016/j.enggeo.2019.105461
[22] Schlosser, F., and L. Dormieux. "Talus et soutènements en dynamique des sols." *Revue française de géotechnique* 37 (1986): 40-60. https://doi.org/10.1051/geotech/1986037040
[23] Mohtarami, E., A. Jafari, and M. Amini. "Stability analysis of slopes against combined circular–toppling failure." *International journal of rock mechanics and mining sciences* 67 (2014): 43-56. https://doi.org/10.1016/j.ijrmms.2013.12.020
[24] Kar, Saurav Shekhar, Anupama Arunkumar Athawale, Avijit Burman, and Lal Bahadur Roy. "Implementing reliability analysis of a soil slope using first-order second moment method, Monte-Carlo simulation method and subset simulation method in a MS-excel spreadsheet." *Journal of Advanced Research in Applied Sciences and Engineering Technology* 36, no. 1 (2023): 176-188. https://doi.org/10.37934/araset.36.1.176188
[25] Giap, Sunny Goh Eng, Amirul Asyraf Zakaria, Mohammad Fadhli Ahmad, Muhammad Zamir Abdul Rasid, Chee-Ming Chan, Mohd Sofiyan Sulaiman, Khasifah Muhamad, Ting Chee Ling, and Hanhan Maulana. "The most likely flooded soil in Terengganu state during historically greatest rainfall intensity." *Journal of Advanced Research in Applied Sciences and Engineering Technology* 41, no. 2 (2024): 152-163. https://doi.org/10.37934/araset.41.2.152163
[26] Belhadj, Kamal, Omar Azzouz, and Makkaoui Mohamed. "Forecast risk maps of land movements in the eastern rif-Morocco." *Materials Today: Proceedings* 45 (2021): 7622-7627. https://doi.org/10.1016/j.matpr.2021.03.101
[27] Kociánová, Lenka, and Rostislav Melichar. "OATools: An ArcMap add-in for the orientation analysis of geological structures." *Computers & Geosciences* 87 (2016): 67-75. https://doi.org/10.1016/j.cageo.2015.12.005